applied sciences

MDPI

Article

CO_2 Snow Cleaning of Red Clay and Starch Deposits on Natural Fibre Textiles: Multi-Analytical Material Response Profiles

Maria Paula Wilches-Cuadros [1,*], Virginia Santamarina-Campos [1,*], Laura Osete-Cortina [2] and Sofía Vicente-Palomino [2]

[1] Department of Conservation and Restoration of Cultural Heritage, Polytechnic University of Valencia, 46022 Valencia, Spain
[2] Heritage Restoration University Research Institute, Polytechnic University of Valencia, 46022 Valencia, Spain; losete@crbc.upv.es (L.O.-C.); svicente@crbc.upv.es (S.V.-P.)
* Correspondence: mpwilcua@upv.es (M.P.W.-C.); virsanca@upv.es (V.S.-C.)

Featured Application

The results provide exploratory data on deposit removal and surface alteration in CO_2 snow cleaning of natural fibre textiles, which can inform the selection of treatment parameters in preliminary cleaning tests.

Abstract

The response of a textile to CO_2 snow cleaning depends on both the nature of the deposit and the structure of the fabric, and its assessment must consider deposit removal together with alteration of the substrate. In this exploratory study, six model systems were prepared by combining three natural fibre textiles (silk, cotton and linen) with a particulate red clay deposit and a gelatinised wheat starch film. Eighteen specimens were characterised before deposit application (M0), after application and drying (M1) and after CO_2 snow treatment (M2), performed using predefined configurations ranging from 1.5 to 6 bar and from 1 to 4 min. Optical measurements followed each specimen through the three states, complemented by surface pH and wettability. In parallel, attenuated total reflectance Fourier transform infrared spectroscopy (ATR-FTIR) provided local spectral characterisation at selected contact sites, while digital and field-emission scanning electron microscopy supplied complementary morphological evidence at different observation scales. The two deposits behaved differently. In the red clay systems, colour recovered partially, with residual colour differences (ΔE*ab) of 6.65 to 34.00 and a persistent reddish and yellowish shift. In the starch systems, low chromatic contrast limited the specificity of colour measurements, while gloss, wetting and microscopy provided complementary evidence. Post-treatment gloss at 85° was below the clean value in 16 of the 18 specimens. Selected FESEM fields showed separated silk filaments and broken cotton fibre ends. These observations identify potential conservation concerns, but their origin and prevalence cannot be established from the available controls and sampling. The results provide exploratory evidence for further evaluation of deposit reduction and textile preservation.

Keywords: CO_2 snow cleaning; textile conservation; silk; cotton; linen; red clay; starch film; attenuated total reflectance Fourier transform infrared spectroscopy (ATR-FTIR); field emission scanning electron microscopy (FESEM)

Check for updates

Academic Editor: Ion Sandu

Received: 29 September 2026
Revised: 20 October 2026
Accepted: 27 October 2026
Published: 4 November 2026

Copyright: © 2026 by the authors. Licensee MDPI, Basel, Switzerland. This article is an open access article distributed under the terms and conditions of the Creative Commons Attribution (CC BY) license.

1. Introduction

Cleaning is one of the most important operations in textile conservation, as the process of removing unwanted material may also affect fibres, yarns, dyes, finishes, or the structural relationships within a fabric. The selection of a cleaning procedure therefore requires consideration not only of the amount of deposit removed, but also of any changes that may be induced in the textile surface. Achieving a suitable balance is particularly challenging when working with porous and heterogeneous materials, as deposited particles may penetrate between fibres and evolve through interactions with the atmosphere and substrate, while the cleaning interventions themselves may affect the optical, mechanical, or surface properties of the textile. Researchers in the area of historical textiles have therefore emphasised the need to assess the efficiency of cleaning and the material response together, rather than treating deposit removal as the sole criterion of suitability [1–5].

The behaviour of a deposit depends on its composition and its interaction with the textile substrate. Mineral particulate deposits may remain on the surface of the fibre or enter the inter-fibre and inter-yarn spaces of the fabric [5]. Starch-based materials behave differently, as they can form cohesive films, adhere to fibres, and alter the optical and surface properties of a fabric. Starch pastes have been used as adhesives or consolidants in textile conservation, and their removal has been investigated mainly through α-amylase-based treatments [6,7]. These studies have shown that the assessment of starch removal must also take into consideration the treatment conditions, residual material, colour, mechanical properties, and possible changes to the fibres [6–8]. Red clay and starch represent two deposits with distinct removal requirements: one mainly consists of particulates, whereas the other can form a continuous or discontinuous film around and between fibres.

Techniques such as mechanical dry cleaning, controlled aqueous treatments, suction-based procedures, and enzymatic methods have been applied to textile materials, according to the characteristics of the object and the deposit [1,2,6,7,9]. However, each procedure has a distinct profile in terms of the interaction with the textile, deposit, and associated materials. In mechanical dry cleaning, physical action may deform or abrade weakened fibres and may displace particles further into a porous structure [5,10]. By contrast, the effectiveness of aqueous cleaning depends on the stability of the fibres, dyes, finishes, and associated materials [1,3]. Enzymatic treatments require careful control over the concentration, pH, temperature, application time, and subsequent removal of the enzyme and degradation products [6,7,11]. These characteristics support the assessment of cleaning processes in which a liquid phase is not directly introduced into the textile. Their evaluation still requires simultaneous documentation of the deposit response and the changes in the optical, surface, and morphological characteristics of the textile [2–4].

In this context, carbon dioxide snow cleaning represents a potentially suitable approach, as it involves passing a stream containing fine solid CO_2 particles generated by the controlled expansion of carbon dioxide through a nozzle [10,12,13]. It must be distinguished from dry ice blasting with macroscopic pellets, as these processes involve different forms of the CO_2 feed, equipment configurations, and operating ranges [14,15]. The smaller mass and dimensions of CO_2 snow particles mean they have a different impact energy from those produced by millimetre-scale pellets [12]. Particle detachment is associated principally with momentum transfer and aerodynamic drag, while the transient formation of liquid CO_2 at the interface may contribute to the removal of some organic residues that are soluble in it [12]. The projected CO_2 subsequently sublimates, so the treatment does not leave particles of the cleaning media on the substrate. However, the mechanical action of the jet and the local decrease in temperature are important aspects when the technique is applied to sensitive fibrous materials [10].

Previous studies have established a basis for considering solid CO_2 cleaning in cultural heritage conservation. Mašková et al. examined the application of CO_2 snow cleaning to paper, and reported the removal of particles from smooth and rough cellulose surfaces, including particles embedded in the fibrous structure. In their evaluation, the cleaning efficiency was investigated via microscopic, optical, mechanical, and chemical observations, and the treatment was compared with nitrogen jet and mechanical dry-cleaning procedures [10]. Stoveland et al. evaluated the use of CO_2 snow blasting and other cleaning systems with artificially aged and soiled painting mock-ups, using visual examination, colour and gloss measurements, light microscopy, and SEM. Their results showed moderate removal of soiling with a comparatively low risk of abrasion, and indicated that surface cooling, condensation, and potential particle redeposition were operational considerations requiring control [16]. Grønlund investigated the use of solid CO_2 blasting for soot removal from fire-affected textiles, and determined its potential for use on less heat-damaged specimens, although that work involved blasting with solid CO_2 rather than the finer snow projection evaluated here [17]. More recently, Mašková et al. assessed the application of automated CO_2 snow microblasting to cellulose-based cultural heritage materials, including uncoated textile surfaces, and compared the response with traditional dry-cleaning methods [18]. Recent experimental work on coated metallic heritage has likewise shown that the cleaning performance of solid CO_2 varies with the target material and substrate–coating system, and that its environmental assessment requires explicit consideration of CO_2 consumption and energy demand [19]. These prior studies show that the technique has already been applied to fibrous heritage materials, but they also highlight that its performance depends on the substrate, contaminant, equipment, operating conditions, and criteria used to identify both cleaning efficacy and alteration.

In the extant literature, the response of CO_2 snow cleaning to deposits with markedly different physical behaviour across natural-fibre textiles remains insufficiently characterised. Heritage applications have focused mainly on particulate contamination of paper and other cellulose-based surfaces, or on the removal of soot from fire-affected textiles using coarser solid CO_2 blasting [17], with limited testing of uncoated textile surfaces [10,18]. Research on other non-contact cleaning techniques also indicates that paper and textile substrates cannot be assumed to behave equivalently, and that the response to a treatment may vary with the chemistry and morphology of the fibre, its age, and the operating parameters [4,20,21]. Few studies have involved direct comparison of a mineral particulate deposit and a film-forming starch deposit applied to silk, cotton, and linen and treated under different CO_2 snow projection conditions. A multi-analytical approach is therefore needed to determine whether apparently similar visual responses are supported by optical, surface, spectroscopic, and morphological evidence [2–4,20].

In this context, the response to CO_2 snow cleaning was compared for six model textile–deposit systems, in which silk, cotton and linen were treated with a particulate red clay deposit or a gelatinised wheat starch film. The treated specimens were examined at three stages, before application of the deposit (M0), after application and drying (M1) and after CO_2 snow treatment (M2). Macroscopic observation and digital microscopy, colourimetry, gloss measurements, surface pH, wettability, attenuated total reflectance Fourier-transform infrared spectroscopy (ATR-FTIR) and field-emission scanning electron microscopy (FESEM) were combined to assess both the removal of the deposits and the response of the textiles.

Given the contrasting physical behaviour of the two deposits, the study aimed to evaluate the extent to which CO_2 snow removed particulate red clay and gelatinised starch from silk, cotton and linen under different pressure and time configurations, and to document the differences observed between the clean, deposited and treated states. The response of each specimen was followed through the sequence M0–M1–M2, and the contribution of

each analytical technique to the assessment of removal and alteration was examined. The study was designed as an exploratory comparison, intended to identify trends and risks that can guide the definition of treatment parameters in future work.

2. Materials and Methods

2.1. Comparative Material-Response Design

This study involved a comparative matrix of material responses, comprising three textiles of natural fibres and two deposits applied in the laboratory. Silk was chosen to represent a proteinaceous substrate, while cotton and linen represented cellulosic substrates. Red clay was selected as a predominantly particulate deposit, and gelatinised wheat starch as a film-forming deposit capable of surrounding fibres and occupying weave interstices.

The basic matrix therefore consisted of six textile–deposit systems. One clean, untreated reference specimen was retained for each textile. Each textile–deposit system included one untreated as-deposited reference, consisting of the textile bearing the dried deposit without CO_2 snow treatment, and the three specimens assigned to the predefined CO_2 snow configurations. Each configuration was therefore applied to a single specimen $(n = 1)$. The complete matrix comprised 27 specimens, namely three clean textile reference specimens, six untreated as-deposited reference specimens, and 18 treated specimens.

The codes SE, AL, and LN were used to represent silk, cotton, and linen, while BA denoted the red clay deposit, and AM denoted starch. The number following each code identified the treatment configuration.

Each treated specimen was characterised in three successive states: M0, corresponding to the clean textile before application of the deposit; M1, representing the same specimen after application and drying of the deposit; and M2, denoting the specimen after CO_2 snow treatment. The clean reference specimens for the textiles were used to establish the initial substrate morphology and spectral profile, while the untreated as-deposited references for the deposits supported the identification of features related to the deposit. Optical measurements followed each treated specimen through the three states. For ATR-FTIR comparisons, spectra from a clean textile reference, an untreated as-deposited reference, and selected treated specimens were used, as described in Section 2.4.

The complete experimental design, coding system, material states, and analytical levels are summarised in Figure 1.

All measurements were referred to the three states defined above. Colour and gloss were measured on every treated specimen at M0, M1 and M2. Surface pH and water-drop absorption were also measured in the three states, with M0 recorded on the clean textile and M1 and M2 on the specimen treated with configuration 3 in each textile–deposit system. The repeated readings taken at each state are technical replicates that describe the variability within a single specimen. The results are therefore reported as exploratory observations on individual specimens rather than as reproducible treatment effects. Qualitative ATR-FTIR comparisons provided local spectroscopic information at selected contact sites, while digital microscopy and FESEM documented the morphological features of selected observation fields. These complementary measurements were integrated according to the direction, magnitude and spatial scale of the information provided by each technique.

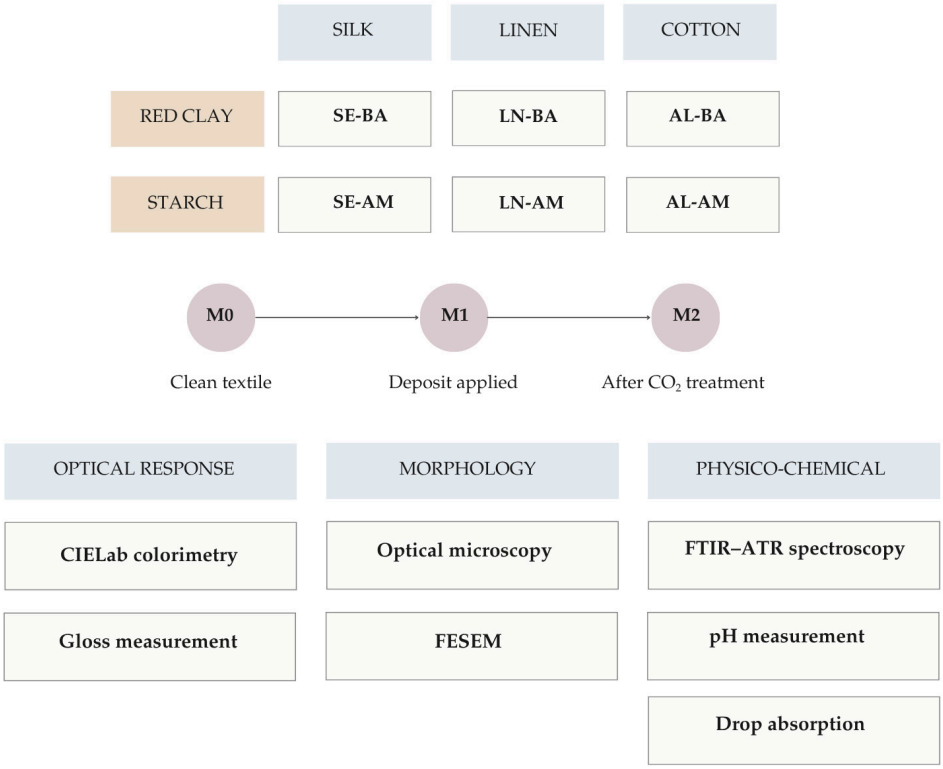


Figure 1. Design of the comparative material response experiment, specimen coding, material states, and analytical levels. In this experimental matrix, silk (SE), cotton (AL), and linen (LN) textiles were combined with either red clay (BA) or starch (AM). M0 denotes the clean textile before application of the deposit, M1 the same specimen after application and drying, and M2 the specimen after CO_2 snow treatment. Results were interpreted based on the specimen trajectory, textile–deposit system, local ATR-FTIR measurement area, and selected microscopy fields.

2.2. Preparation of Textile–Deposit Model Systems

The substrates were commercial undyed fabrics made of silk, cotton, and linen. Their suppliers and commercial references are given in Table 1.

Table 1. Characteristics of the textile substrates.

Property	Silk Habotai 10	Batista Cotton	Linen CTS 2139
Supplier	Sodintex® natural fibres	Productos de Conservación, S.A.	C.T.S. España S.L.
Commercial reference	Seda Habotai 10	Batista de algodón 100%. Ref 00293	TELA ART. CTS 2139—100% LINO
Composition	100% silk	100% cotton	100% linen
Mass per unit area (g/m²)	45	127	115
Weave	Plain weave	Plain weave	Plain weave
Thread density, warp × weft, (threads/cm)	40 × 50	30 × 45	13 × 13
Twist direction	n.a.	Z	Z
Twist angle	n.a.	35°	15°

Note: n.a.: not applicable. The silk yarns were untwisted, and no twist angle or direction was therefore assigned. Mass per unit area as stated by the manufacturer. Twist angles were estimated on digital micrographs relative to the yarn axis.

Before preparation of the specimens, the fabrics were prewashed in an aqueous Teepol solution at 2 mL/L to remove manufacturing finishes that could interfere with the initial characterisation or subsequent measurements. The prewashed fabrics were subsequently

air-dried horizontally at room temperature, and then cut along the thread directions into specimens measuring 75 × 100 mm. Each specimen was individually coded, and the same identifier was retained throughout preparation, treatment, and analysis.

The red clay deposit was prepared by dispersing SIO-2 Argila natural red clay in water at 100 g/L. Specimens were immersed in the dispersion for 5 min and then dried on a rigid support for approximately 24 h, under ambient laboratory conditions. Drying was considered complete when the aqueous medium had visibly evaporated and the specimens had reached an apparently dry state.

The starch deposit was prepared using commercial wheat starch supplied by CTS Europe, Altavilla Vicentina, Italy. Two predefined material protocols were used, 5% w/v for silk and cotton and 10% w/v for linen. The higher concentration was chosen for linen to obtain a more evident surface film on its more open weave, which has a much lower thread density than the other two fabrics (Table 1). During preparation, the recorded temperature ranged from approximately 60 to 75 °C. The starch dispersions were heated for 5–10 min with continuous manual stirring. Gelatinisation was considered complete when the paste took on a homogeneous, creamy, and translucent appearance after the maximum observed viscosity had been reached. The specimens were immersed in the prepared paste and immediately withdrawn, without an extended immersion period. They were subsequently dried on a rigid support to limit planar deformation during the water loss and film formation processes. Since the applied formulation differed between the linen fabric and the silk and cotton specimens, each textile–starch system was analysed within its own predefined conditions, and cross-system interpretation focused on analytical response patterns rather than on absolute magnitudes.

In both series, the face in contact with the support was taken as the reverse. CO_2 snow was applied to the opposite (front) face, on which all measurements were taken. The interval between deposit application and CO_2 snow treatment was not recorded.

2.3. CO_2 Snow Treatment

CO_2 snow was applied using a CryoSnow SJ-5 system fitted with a flat nozzle (FN-5-10 × 1.5). The nozzle had a rectangular outlet measuring 10 × 1.5 mm [22]. The system was operated manually using the trigger, and the jet was moved across the surface of the specimen with a sweeping motion.

Treatments were applied in the cryogenic testing area of the CMT-Clean Mobility & Thermofluids Institute, Universitat Politècnica de València. The recorded environmental conditions were 25 °C and 50% relative humidity. The nozzle was held at an incident angle of 45°, and the working distance was maintained between 20 and 30 mm from the textile surface.

The equipment, nozzle, and application geometry are shown in Figure 2.

The treatment matrix comprised the configurations listed in Table 2, which were defined according to the response of each textile–deposit system and were not designed as a factorial study. For the red clay series, a fixed application time of 1 min was used, with nominal pressure settings adjusted to each textile and starting at lower values for the lightweight silk. Longer application times were used for the starch series. The linen–starch series involved application times of 2, 3 and 4 min at a nominal setting of 6 bar, whereas the silk–starch and cotton–starch series combined different pressure and time settings. Each pressure–time combination was therefore treated as a complete operational configuration, and the results cannot be attributed to pressure or application time as independent variables. Treatment of each specimen ceased when the cumulative application time assigned in Table 2 had elapsed.



(**a**) (**b**) (**c**)

Figure 2. CryoSnow SJ-5 system, flat nozzle, and geometry used to apply CO_2 snow. (**a**) CryoSnow SJ-5 equipment; (**b**) manual sweeping over the 75 × 100 mm specimen at an angle of incidence of 45° and a working distance of 20–30 mm; (**c**) FN-5-10 × 1.5 flat nozzle with a rectangular outlet measuring 10 × 1.5 mm [22,23].

Table 2. CO_2 snow treatment conditions.

Deposit	Textile	Specimen	Nominal Pressure Setting (bar)	Cumulative Application Time (min)
Red clay	Silk	SE-BA1	1.5	1
Red clay	Silk	SE-BA2	2.5	1
Red clay	Silk	SE-BA3	5	1
Red clay	Cotton	AL-BA1	2	1
Red clay	Cotton	AL-BA2	3	1
Red clay	Cotton	AL-BA3	5	1
Red clay	Linen	LN-BA1	2	1
Red clay	Linen	LN-BA2	4	1
Red clay	Linen	LN-BA3	5	1
Starch	Silk	SE-AM1	6	2
Starch	Silk	SE-AM2	5	2
Starch	Silk	SE-AM3	3	3
Starch	Cotton	AL-AM1	5	2
Starch	Cotton	AL-AM2	6	2
Starch	Cotton	AL-AM3	6	3
Starch	Linen	LN-AM1	6	2
Starch	Linen	LN-AM2	6	3
Starch	Linen	LN-AM3	6	4

Note: Pressure values correspond to the nominal equipment settings used during treatment, and do not represent pressure measurements at the textile surface. Application time denotes the cumulative treatment time over the defined test area.

The pressure values given below correspond to nominal CryoSnow SJ-5 equipment settings, rather than to pressure measurements at the textile surface [22]. According to the manufacturer, the SJ-5 system has overall consumption rates of 0.10–0.25 m^3 min^{-1} for compressed air and 0.04–0.08 kg min^{-1} for liquid CO_2. For the FN-5-10 × 1.5 nozzle used in this study, the manufacturer reports a compressed air consumption rate of 0.20 m^3 min^{-1} at 6 bar [23]. Based on the liquid CO_2 consumption rate, the nominal CO_2 consumption per unit area ranged from approximately 0.5 to 4.3 g cm^{-2} across the matrix. Because the jet was swept manually, the local dose at any point of the specimen was not defined.

The treated area and general mode of application were kept constant across all treatment conditions. The jet was moved continuously in a manual sweeping motion across the full exposed face of each 75 × 100 mm specimen (75 cm^2) for the cumulative application time specified in Table 2, rather than in a predefined sequence of discrete passes.

Surface temperature was monitored during treatment using a thermocouple in contact with the reverse side of the specimen and positioned within the area affected by the jet. The readings therefore represent the transmitted thermal response at the monitored location on the reverse side, rather than the temperature of the CO_2 stream or of the directly exposed textile surface. The temperature values recorded during treatment are reported in Section 3.1.

The tests were carried out in a ventilated room with local extraction operating throughout the session. Ambient CO_2 was monitored using a DioxCare sensor in addition to the detector incorporated into the equipment. Gloves for thermal protection and safety glasses were worn to reduce the risks associated with cold surfaces, accidental contact with the jet, and projected particles.

2.4. Analytical Characterisation

The specimens were examined using complementary optical, morphological, physicochemical, and spectroscopic techniques. The analytical methods, equipment, and measurement scope are summarised in Table 3.

Table 3. Analytical techniques used to characterise the specimens.

Analytical Technique/Test	Equipment	Analytical Level	Procedure and Analytical Output
Digital microscopy	Dino-Lite Digital Microscope Premier	Selected microscopy field	Examination of textile morphology, weave, thread density, twist, deposit distribution, and local surface-response features in selected fields at M0, M1, and M2
CIELAB Colourimetry	CHN Spec CS-10	Specimen trajectory	Measurements in the CIE L*a*b* (CIELAB) colour space, with five readings per specimen at each state, following the principles of UNE-EN 15886:2011 [24]
Specular gloss measurement	Konica Minolta Multi Gloss 268A	Specimen trajectory	Measurements at 85° for all specimens and at 60° for the starch systems, consisting of five readings per specimen in each state, with the 85° geometry prioritised due to the low-gloss nature of the textile surfaces
Surface pH measurement	HORIBA LAQUAtwin-pH-22	Textile–deposit system	Surface pH measured indirectly using a fragment of agarose gel placed in contact with the textile for 3 min [25]; four readings obtained for each reported textile–deposit state

Table 3. *Cont.*

Analytical Technique/Test	Equipment	Analytical Level	Procedure and Analytical Output
Water drop wetting test	Labbox EASY 40 Elite micropipette for droplet dispensing	Textile–deposit system	Comparative assessment using 10 µL droplets of distilled water; initial apparent contact angle and total absorption time recorded to assess the wetting behaviour of each textile–deposit system across a series of four readings for each reported textile–deposit state, using a procedure informed by UNE-EN 15802:2010 [26]
Attenuated total reflectance Fourier-transform infrared spectroscopy (ATR-FTIR)	Bruker ALPHA II Compact FT-IR spectrometer with monolithic diamond ATR crystal	ATR contact site	Spectra recorded in absorbance mode over 4000–500 cm^{-1} at 4 cm^{-1} resolution, with 24 scans per spectrum; qualitative comparison of spectra acquired at selected contact sites on separate clean-reference, untreated deposited-reference and treated specimens.
Field-emission scanning electron microscopy (FESEM)	Zeiss Ultra 55 with SE2 detector	Selected microscopy field	Uncoated specimens examined at an accelerating voltage of 1.00 kV and working distances ranging from 3.1 to 3.5 mm, depending on the image; fibre-scale surface morphology documented in selected fields.

Note: Analytical level represents the scale at which the results from each technique were interpreted.

Colour differences were calculated using the CIE76 formula given in Equation (1) [24]. The M1–M0 comparison described the chromatic change associated with the application of the deposit, while M2–M0 expressed the residual difference between the treated specimen and its initial clean state. Five colour readings were distributed across the defined measurement area in each state, with the specimen placed on a black background that was kept the same in all states, and were averaged for each specimen.

$$\Delta E^*_{ab} = \sqrt{(\Delta L^*)^2 + (\Delta a^*)^2 + (\Delta b^*)^2} \quad (1)$$

Gloss measurements were obtained at 85° for all specimens and at 60° for the starch systems, with reference to the geometries defined in UNE-EN ISO 2813:2015 [27]. As this standard was developed for non-textured coatings on plane, opaque substrates, the resulting gloss units were interpreted as comparative surface measurements within the experimental sequence, rather than as fully standardised absolute gloss values for textiles. Gloss readings were intended to be taken in a constant orientation, with the specimen positioned with the weft horizontal. Because the gloss of textiles is anisotropic, small changes in orientation between specimens cannot be excluded and may contribute to the variability of the clean-state values. Readings below 1 GU at 85° approach the lower limit of the gloss scale and were interpreted as indicating very low gloss rather than as precise values.

The water droplet response was described through the initial apparent contact angle and total absorption time. These values correspond to apparent angles on a porous fabric and not to static contact angles in the sense of the standard. Cases in which the droplet was absorbed before a stable apparent angle could be measured were recorded as immediate absorption (<1 s) and were not assigned an angle of 0°.

ATR-FTIR spectra were acquired without baseline correction and were used for qualitative comparison of selected contact sites. One spectrum was acquired at a central contact

site on each analysed specimen. The comparisons included the clean textile reference, the untreated as-deposited reference and two selected treated specimens per textile–deposit system. The treated specimens were SE-BA2, SE-BA3, LN-BA2, LN-BA3, AL-BA2, AL-BA3, SE-AM2, SE-AM3, LN-AM1, LN-AM3, AL-AM1 and AL-AM3. These spectra correspond to separate specimens rather than paired M1–M2 measurements. Differences in deposit coverage, specimen–crystal contact and overlapping bands limit quantitative comparisons. No percentage of deposit removal was calculated from the spectra [28].

FESEM was used to complement the interpretation of the surface response with morphological evidence at the fibre scale. For each textile–deposit system, the clean textile reference, the untreated as-deposited reference and the specimen treated with configuration 3 were examined, the latter being the same specimen used for surface pH and wetting. Three to four fields were examined on each specimen, and representative fields were selected for presentation in Section 3.4.

2.5. Data Analysis

Colour, gloss and surface pH readings were summarised as the mean and standard deviation for each specimen and state, and wetting results as mean values. ΔE*ab was calculated from the mean colour coordinates. Its reported dispersion was estimated by propagation of the coordinate standard deviations and is not the standard deviation of five independently calculated colour differences. Because each configuration was applied to a single specimen, no inferential statistical tests were performed, and comparisons between configurations are descriptive. ATR-FTIR spectra were compared qualitatively, without calculating removal percentages or ranking treatment configurations. Digital microscopy documented the weave and the distribution of the deposit in selected fields, and FESEM documented the surface of individual fibres at higher magnification.

3. Results

The results are presented for each treated specimen across the three states M0, M1, and M2. Tables 4 and 5 give the colour and gloss measurements for each configuration of the red clay and starch systems, respectively. ATR-FTIR results are reported as spectral responses at the contact site and are interpreted together with the corresponding microscopy observations.

Table 4. Colour difference and gloss of the red clay specimens (mean ± SD). Gloss values were measured at 85°. All red-clay specimens underwent CO_2 snow cleaning for 1 min.

Specimen	Nominal Pressure Setting (bar)	ΔE*ab M1–M0	ΔE*ab M2–M0	Gloss at 85°, GU		
				M0	M1	M2
SE-BA1	1.5	37.55 ± 0.78	34.00 ± 0.78	10.90 ± 0.81	3.54 ± 1.01	0.54 ± 0.09
SE-BA2	2.5	39.48 ± 2.44	30.05 ± 1.44	10.42 ± 1.29	2.44 ± 0.67	0.54 ± 0.05
SE-BA3	5	42.61 ± 2.93	20.42 ± 0.63	10.58 ± 1.01	2.62 ± 1.43	0.26 ± 0.29
LN-BA1	2	25.34 ± 1.60	27.61 ± 1.30	2.80 ± 1.33	3.02 ± 1.34	0.90 ± 1.57
LN-BA2	4	24.49 ± 1.45	6.65 ± 0.70	4.80 ± 0.82	2.24 ± 1.83	0.70 ± 0.07
LN-BA3	5	26.82 ± 1.06	6.83 ± 0.67	2.72 ± 1.07	2.76 ± 0.47	0.58 ± 0.08
AL-BA1	2	43.92 ± 2.04	20.49 ± 1.14	4.02 ± 0.31	2.94 ± 1.61	0.68 ± 0.18
AL-BA2	3	45.46 ± 0.74	21.77 ± 1.99	4.28 ± 0.88	3.18 ± 1.51	0.80 ± 0.10
AL-BA3	5	44.39 ± 0.68	16.76 ± 0.68	5.10 ± 0.84	3.68 ± 1.69	0.82 ± 0.13

Note: Gloss values are means ± SD of the readings taken on a single specimen. For ΔE*ab, the dispersion was obtained by propagation of the standard deviations of L*, a* and b* (Section 2.5).

Table 5. Colour difference and gloss at 85° and 60° (mean ± SD) of the starch systems.

Specimen	Nominal Pressure Setting and Application Time	ΔE*ab M1–M0	ΔE*ab M2–M0	Gloss at 85°, (GU), M0	Gloss at 85°, (GU), M1	Gloss at 85°, (GU), M2	Gloss at 60°, (GU), M0	Gloss at 60°, (GU), M1	Gloss at 60°, (GU), M2
SE-AM1	6 bar, 2 min	1.49 ± 0.30	1.52 ± 0.40	11.12 ± 0.88	13.04±0.61	2.20 ± 0.92	3.2 ± 0.1	5.7 ± 0.2	3.1 ± 0.2
SE-AM2	5 bar, 2 min	0.98 ± 0.51	1.70 ± 0.41	10.38 ± 0.71	12.54 ± 1.51	1.18 ± 0.76	3.2 ± 0.1	5.0 ± 0.5	2.9 ± 0.3
SE-AM3	3 bar, 3 min	1.61 ± 0.56	2.22 ± 0.40	11.42 ± 0.35	9.94 ± 1.72	1.68 ± 0.43	3.3 ± 0.0	3.5 ± 0.3	2.9 ± 0.3
LN-AM1	6 bar, 2 min	1.81 ± 1.54	1.81 ± 1.07	3.24 ± 0.77	24.14 ± 3.01	8.42 ± 4.00	1.4 ± 0.0	17.5 ± 3.3	6.3 ± 3.8
LN-AM2	6 bar, 3 min	1.41 ± 1.69	1.97 ± 1.69	3.42 ± 0.97	21.98 ± 2.70	7.70 ± 1.72	1.4 ± 0.0	15.3 ± 2.4	6.5 ± 0.9
LN-AM3	6 bar, 4 min	1.37 ± 1.30	2.88 ± 1.55	3.78 ± 0.52	17.70 ± 2.04	3.26 ± 1.18	1.5 ± 0.0	8.6 ± 1.5	3.5 ± 1.0
AL-AM1	5 bar, 2 min	0.76 ± 0.78	2.26 ± 0.64	11.50 ± 2.03	11.62 ± 3.40	2.98 ± 2.31	3.0 ± 0.1	4.6 ± 1.2	3.8 ± 1.0
AL-AM2	6 bar, 2 min	0.69 ± 0.70	0.21 ± 0.46	10.96 ± 0.85	9.88 ± 4.46	0.98 ± 0.26	3.0 ± 0.0	4.2 ± 1.2	2.6 ± 0.2
AL-AM3	6 bar, 3 min	0.33 ± 0.43	1.37 ± 0.40	3.92 ± 0.63	10.44 ± 2.75	0.60 ± 0.25	3.0 ± 0.0	4.2 ± 0.7	2.6 ± 0.2

Note: Gloss values are means ± SD of the readings taken on a single specimen. For ΔE*ab, the dispersion was obtained by propagation of the standard deviations of L*, a* and b* (Section 2.5).

3.1. Treatment Temperature Profile

The temperature was monitored on the reverse side of the area affected by the jet. A minimum of 0.7 °C was recorded under direct impact of the jet, while temperatures during manual sweeping remained between 8 and 10 °C. After application ceased, the temperature of the monitored area returned rapidly towards ambient.

3.2. Red Clay

The responses for the red clay systems are described based on post-treatment digital microscopy, colourimetry, gloss measurements at 85°, ATR-FTIR comparisons, surface wetting behaviour, and surface pH. Digital microscopy was used to document the residual deposit distribution and local textile morphology after CO_2 snow cleaning, while the remaining measurements characterised the M0–M1–M2 response of each textile–deposit system.

In the post-treatment digital microscopy fields, SE-BA2 and SE-BA3 showed wider interthread spacing than SE-BA1, together with differences in the visible coverage of residual deposits. The LN-BA3 field showed larger interstices and less orthogonal weave alignment than the LN-BA1 and LN-BA2 fields. The three cotton fields showed differences in residual red clay coverage, without visible thread displacement. The digital microscopy fields recorded after treatment are shown in Figure 3.

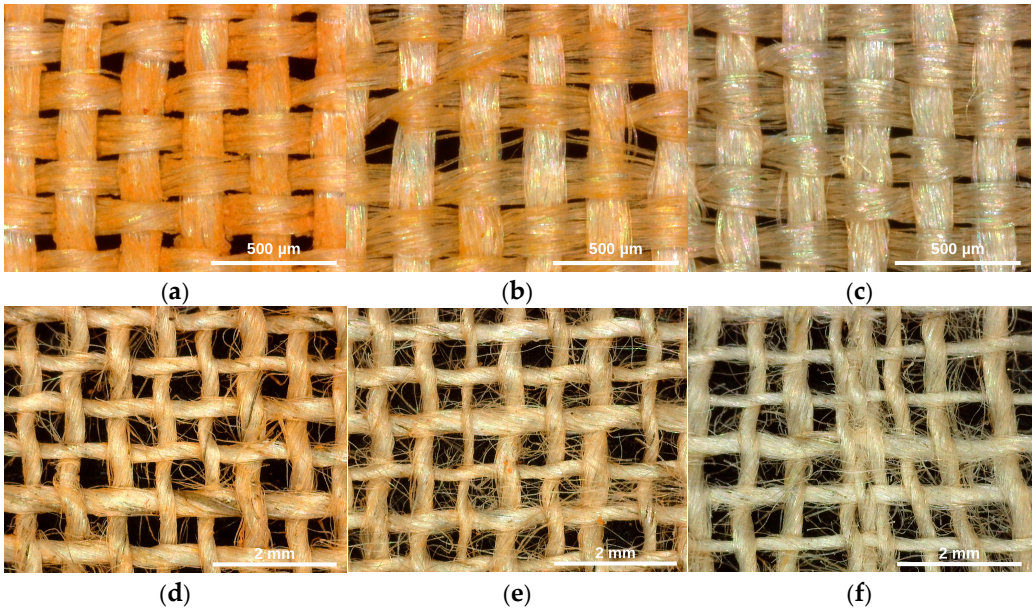
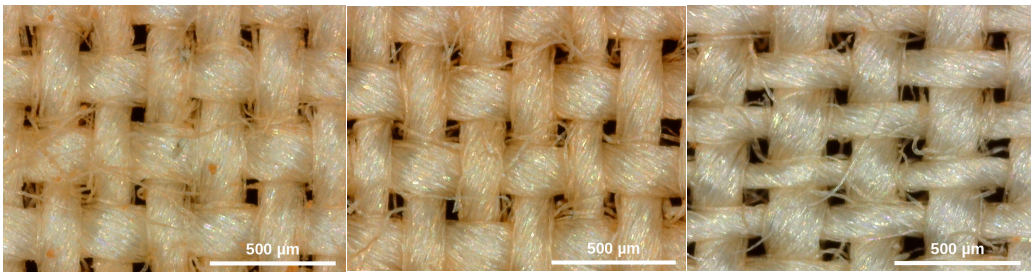


Figure 3. *Cont.*



(**g**) (**h**) (**i**)

Figure 3. Post-treatment (M2) digital microscopy fields for the red clay textile systems across the tested CO_2 snow configurations: (**a**–**c**) silk, SE-BA1, SE-BA2, and SE-BA3; (**d**–**f**) linen, LN-BA1, LN-BA2, and LN-BA3; (**g**–**i**) cotton, AL-BA1, AL-BA2, and AL-BA3. The corresponding treatment conditions are listed in Table 2.

The colourimetric measurements characterised the M0–M1–M2 responses for the clay systems, with colour differences expressed as ΔE*ab, as shown in Table 4. For silk, the M1–M0 ΔE*ab values associated with application of the red clay deposit ranged from 37.55 to 42.61. After treatment with CO_2 snow, the corresponding M2–M0 ΔE*ab values were 34.00 for SE-BA1, 30.05 for SE-BA2 and 20.42 for SE-BA3. For linen, the M1–M0 and M2–M0 ΔE*ab values were 25.34 and 27.61 for LN-BA1, 24.49 and 6.65 for LN-BA2, and 26.82 and 6.83 for LN-BA3, respectively. For cotton, the M1–M0 ΔE*ab values ranged from 43.92 to 45.46, whereas the M2–M0 ΔE*ab values ranged from 16.76 to 21.77. In LN-BA1, the colour after treatment remained close to that of the deposited state, indicating no chromatic recovery towards M0. In every red clay specimen showing chromatic recovery, b* was the coordinate that recovered least, and residual positive shifts in a* and b*, towards red and yellow, persisted after treatment. Recovery of L* exceeded that of a* in cotton and linen, whereas in silk it was lower than or similar to that of a* (Table S2).

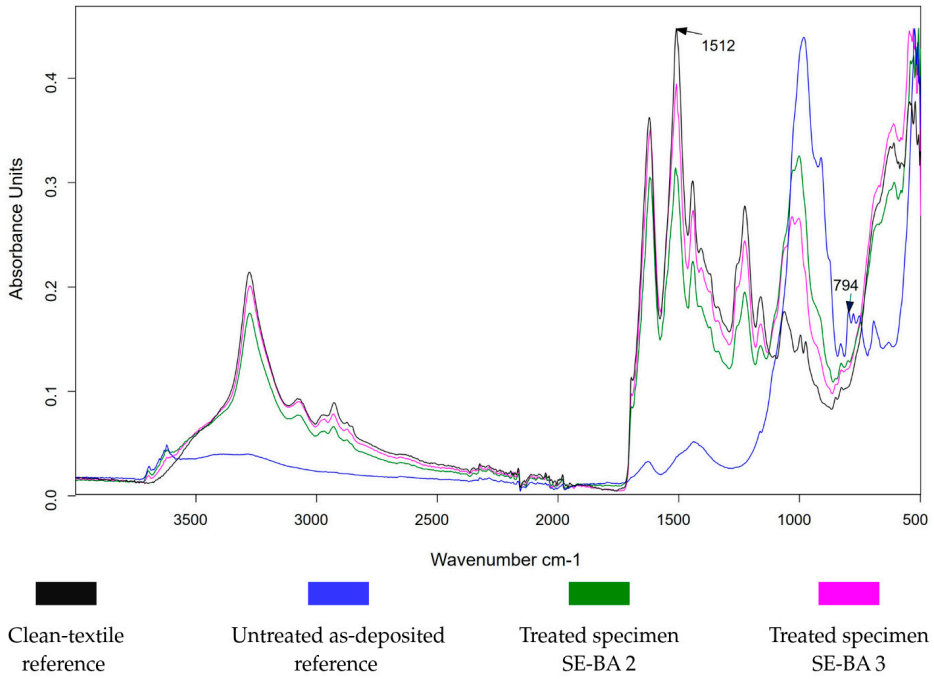
Gloss measurements at 85° showed a decrease in the M2 values compared with both M0 and M1 for all clay-treated specimens. For the silk specimens, the gloss decreased from M0 values of 10.42–10.90 GU to 0.26–0.54 GU at M2, whereas for linen, the values decreased from 2.72–4.80 GU to 0.58–0.90 GU, and for cotton, they decreased from 4.02–5.10 GU to 0.68–0.82 GU. All values after treatment were below 1 GU.

ATR-FTIR analysis provided complementary spectroscopic information on selected contact sites. The principal textile-associated bands remained identifiable in the treated specimens. The feature near 794 cm^{-1} was considered a quartz-associated feature of the commercial mineral deposit rather than a specific indicator of its complete clay fraction. The comparative spectra are shown in Figure 4.

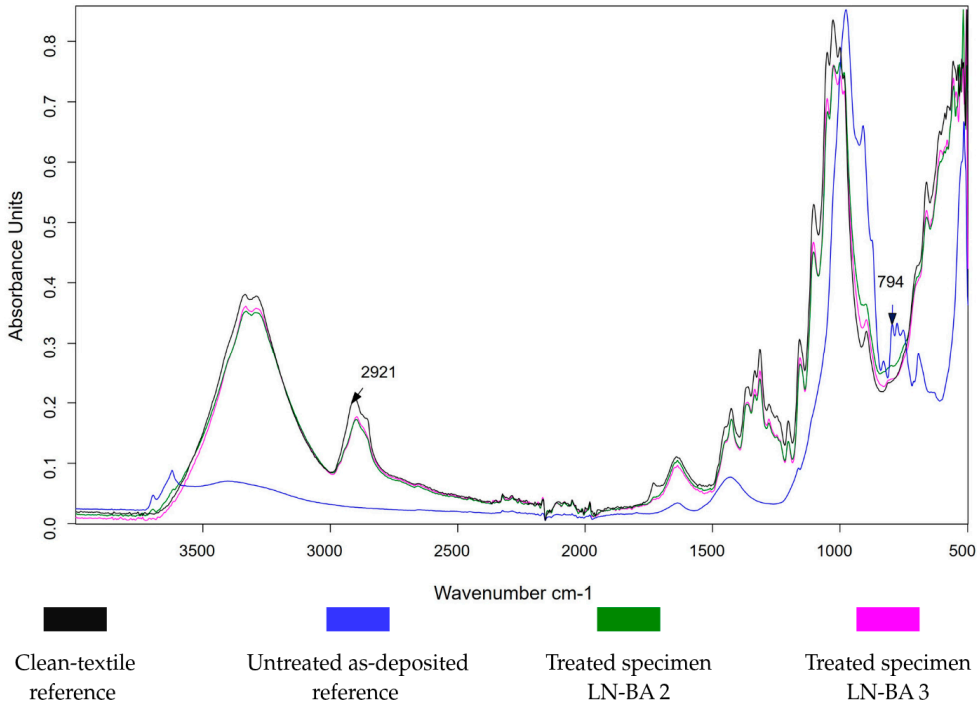
The surface wetting behaviour of the red clay systems also differed among the substrates. On silk, the clean textile produced an initial apparent contact angle of 78.36° and absorbed the drop within 3 s. Both the M1 and M2 specimens absorbed the drop immediately, preventing the formation of a stable contact angle. For linen, the values changed from 81.38° and 9 s at M0 to immediate absorption at M1, and 73.31° and 3 s at M2. For cotton, the values changed from 98.23° and 300 s at M0 to immediate absorption at M1, followed by 79.43° and 5 s at M2.

Finally, surface pH was 8.53 ± 0.14 for clean silk, 8.85 ± 0.19 for clean cotton and 8.87 ± 0.19 for clean linen. After application of the red clay, values of 7.79 ± 0.15 for silk, 7.84 ± 0.10 for linen and 7.79 ± 0.23 for cotton were recorded, and after treatment the values were 7.66 ± 0.15, 7.85 ± 0.18 and 7.78 ± 0.12, respectively. The decrease relative to the clean textiles was therefore already present before treatment, and the differences between the deposited and treated states, between −0.13 and +0.01 pH units, were within the standard

deviation of the readings. These measurements describe the tested surface locations, and do not characterise the complete treated area.

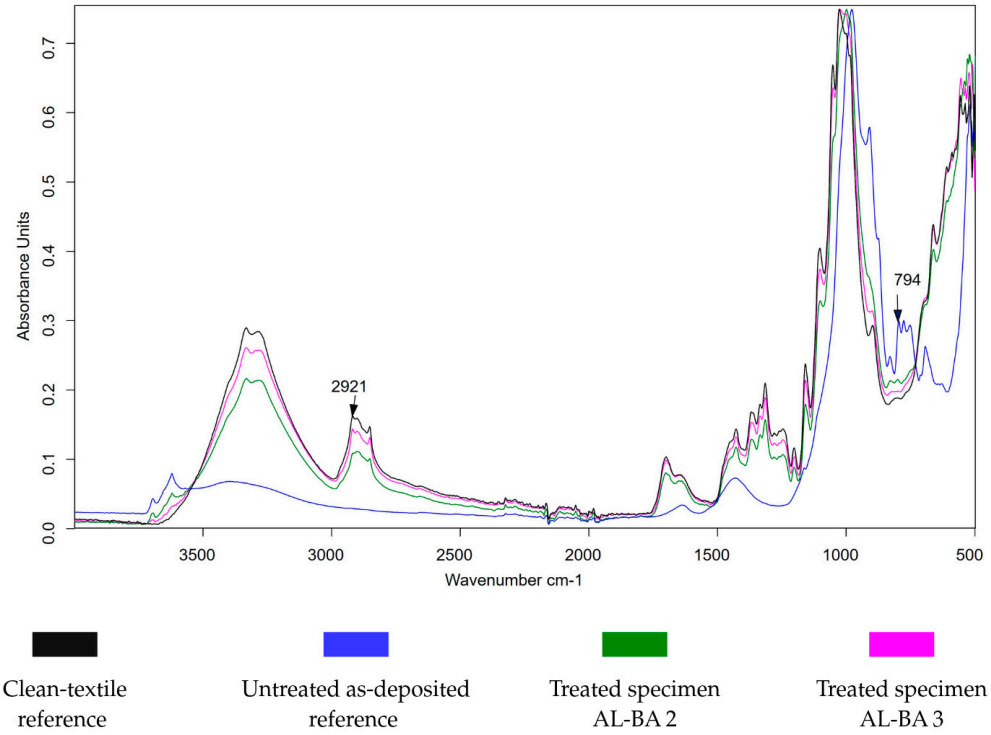


(**a**)



(**b**)

Figure 4. *Cont.*



(**c**)

Figure 4. ATR-FTIR spectra recorded at selected contact sites for the red clay–textile systems. Panels show (**a**) silk, (**b**) linen, and (**c**) cotton. The spectra correspond to the clean textile reference, untreated as-deposited reference, and treated specimens (identified by code in the legend). The quartz-associated feature of the mineral deposit (near 794 cm^{-1}) and the substrate-associated bands (near 1512 cm^{-1} for silk and 2921 cm^{-1} for linen and cotton) are indicated.

3.3. Starch

The response of the starch systems was evaluated by integrating the colour, gloss, wettability, surface pH, ATR-FTIR, and microscopy data. In contrast to the red clay systems, the gelatinised starch films produced limited visual and chromatic contrast with the textile substrates. Interpretation of these systems therefore relied not only on colour differences but also on surface-sensitive measurements, local spectroscopic information, and morphological observations of residual film distribution.

Colour difference and gloss values for the starch systems are reported in Table 5. The starch films generated low chromatic contrast, with ΔE*ab values between 0.33 and 1.81 for M1–M0 and between 0.21 and 2.88 for M2–M0 across the nine specimens. This limits the specificity of colour differences for assessing residual starch.

Post-treatment digital microscopy was used to document the distribution of residual starch film and local textile morphology. In the silk–starch systems, the digital microscopy field at ×50 for SE-AM2 showed areas with variable interthread spacing, while the ×200 field showed material remaining on the yarn surfaces. The fields for LN-AM1, LN-AM2, and LN-AM3 displayed differences in the visible distribution of the surface film. For cotton, the fields showed aligned threads, without visible displacement. Post-treatment digital microscopy fields are shown in Figure 5.

Gloss measurements provided a more sensitive assessment of the application of starch and of the treatment than colour measurements. At 85°, the M2 readings for all nine starch-treated specimens fell below their respective M1 values. The relationship between M2 and M0 varied by substrate. On silk, M2 values ranged from 1.18 to 2.20 GU, well below the

M0 values of 10.38–11.42 GU. At 60°, M2 values ranged from 2.9 to 3.1 GU, close to the M0 values of 3.2–3.3 GU.

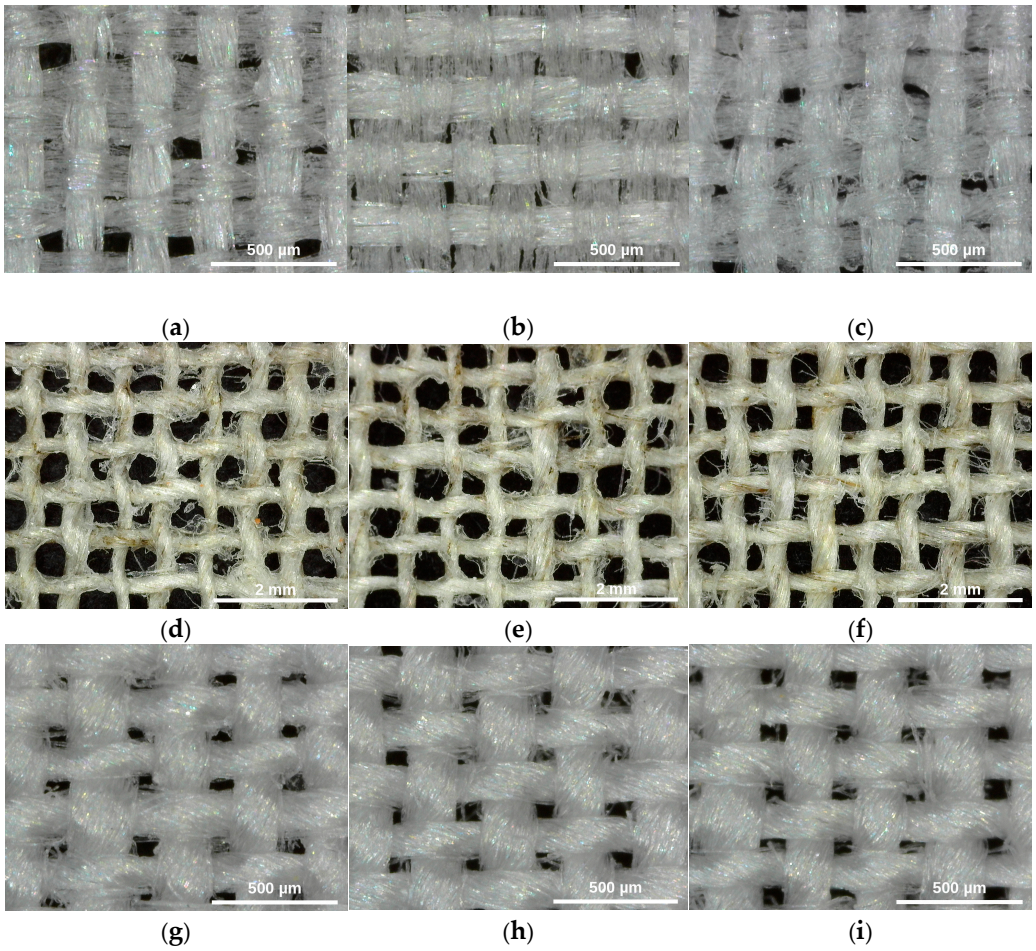


Figure 5. Post-treatment (M2) digital microscopy fields of the starch textile systems across the tested CO_2 snow configurations. (**a**–**c**) silk, SE-AM1, SE-AM2, and SE-AM3; (**d**–**f**) linen, LN-AM1, LN-AM2, and LN-AM3; (**g**–**i**) cotton, AL-AM1, AL-AM2, and AL-AM3. The corresponding treatment conditions are reported in Table 2.

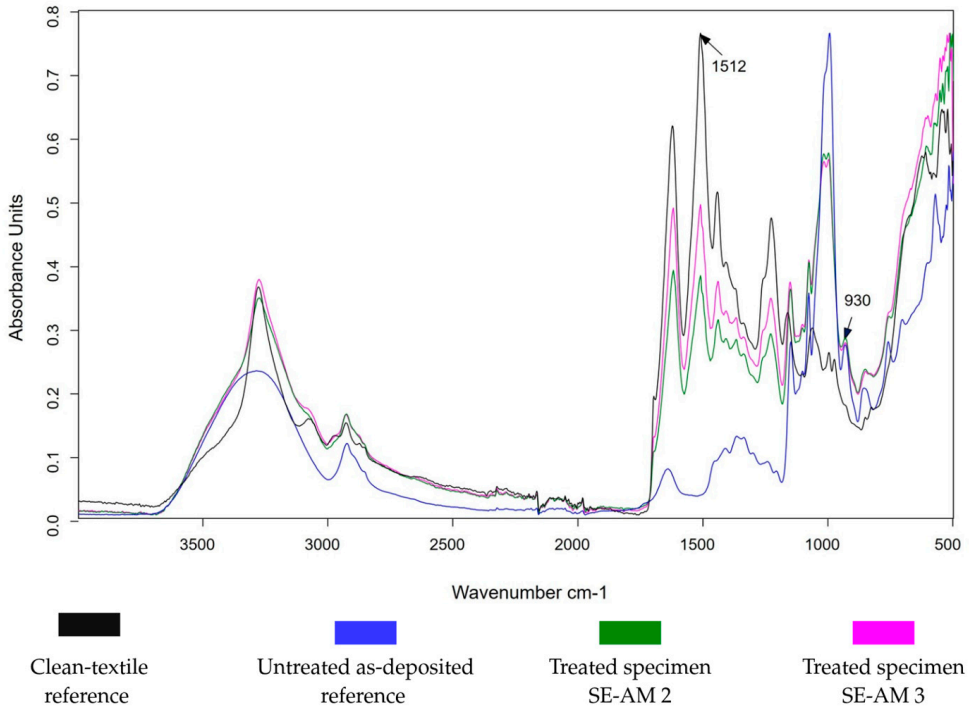
For the linen specimens, there was a marked increase in gloss after the application of starch. At 85°, M1 values ranged from 17.70 to 24.14 GU, compared with M0 values of 3.24–3.78 GU. After treatment, the M2 results for LN-AM1 and LN-AM2 remained above their respective M0 values, at 8.42 and 7.70 GU, whereas LN-AM3 reached 3.26 GU, slightly below its M0 value. At 60°, M0 values ranged from 1.4 to 1.5 GU, M1 values from 8.6 to 17.5 GU, and M2 values from 3.5 to 6.5 GU. All three M2 readings therefore remained above their respective M0 values.

For cotton, the clean-state readings at 85° varied between specimens. In all three specimens, the value after treatment was lower than both the clean and deposited values. At 60°, the M2 value for AL-AM1 reached 3.8 GU, compared with 3.0 GU at M0, while for AL-AM2 and AL-AM3, M2 reached 2.6 GU, slightly below the M0 value of 3.0 GU.

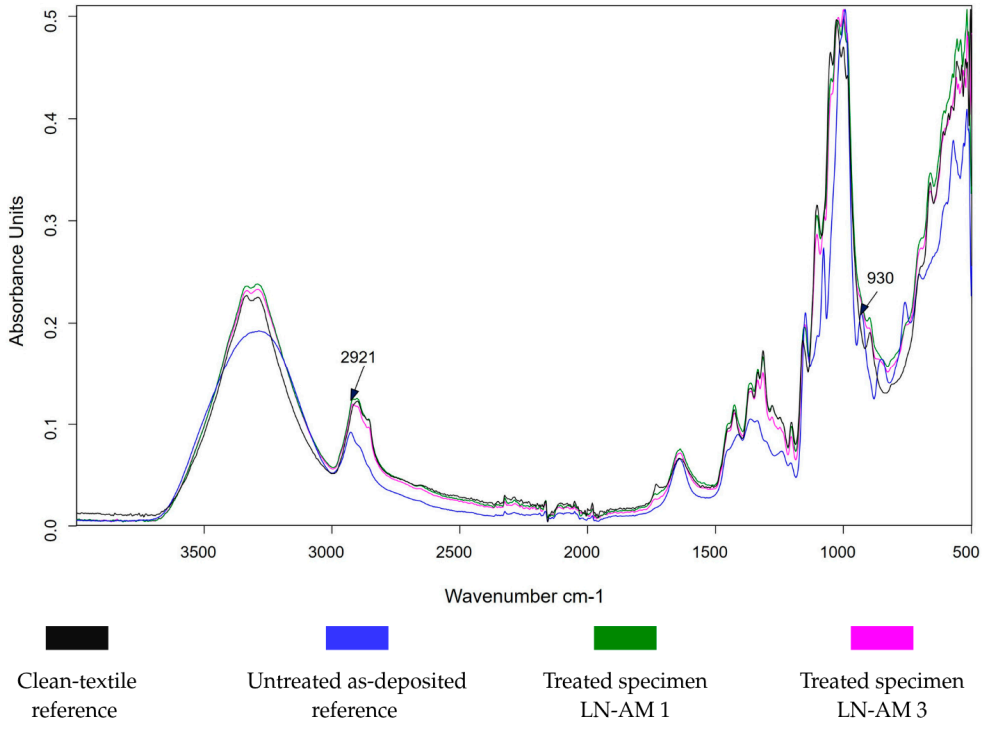
ATR-FTIR analysis provided local spectroscopic information on selected contact sites. Overlapping starch and cellulose bands limited the specificity of spectral comparisons in cotton and linen. The principal textile-associated bands remained identifiable in the treated specimens. The comparative spectra are shown in Figure 6.

Differences in the surface wetting behaviour were also found among the textile–starch systems. For silk–starch, the apparent contact angle and absorption time changed from

78.36° and 3 s at M0 to 78.38° and 9 s at M1, followed by 77.15° and 7 s at M2. For linen, these values changed from 81.38° and 9 s at M0 to 84.55° and 20 s at M1, followed by 78.54° and 3 s at M2. For cotton, the changes were from 98.23° and 300 s at M0 to 75.51° and 90 s at M1, followed by 83.28° and 150 s at M2.

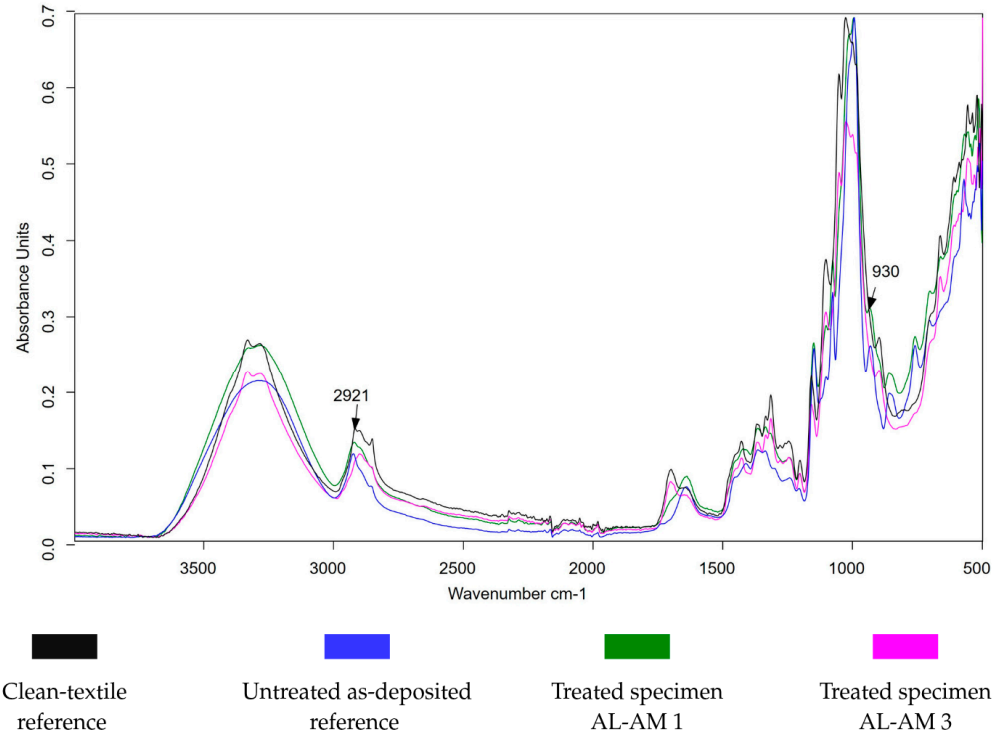


(**a**)



(**b**)

Figure 6. *Cont.*



(**c**)

Figure 6. ATR-FTIR spectra recorded at selected contact sites of the starch textile systems. Panels show results for (**a**) silk, (**b**) linen, and (**c**) cotton. The spectra correspond to the clean textile reference, untreated as-deposited reference, and treated specimens (identified by code in the legend). The starch-associated band (near 930 cm^{-1}) and the substrate-associated bands (near 1512 cm^{-1} for silk and 2921 cm^{-1} for linen and cotton) are indicated.

Finally, surface pH after application of the starch was 7.56 ± 0.19 for silk, 7.64 ± 0.05 for linen and 7.60 ± 0.08 for cotton, and after treatment it was 7.74 ± 0.10, 7.86 ± 0.10 and 7.77 ± 0.14, respectively. As in the red clay systems, the values were already lower than those of the clean textiles before treatment (Section 3.2). The treated states showed small increases of 0.16 to 0.22 pH units relative to the deposited states, and in neither series was persistent acidification detected after treatment at the tested sites.

3.4. Morphological Observations

Digital microscopy and FESEM provided complementary morphological documentation of surface features and weave structure at different spatial scales. The digital microscopy results showed the deposit distribution and weave-level response in the red clay and starch systems (Figures 3 and 5, respectively), whereas FESEM resolved the local surface morphology within selected fields corresponding to the reference, deposited, and treated states (Figures 7 and 8, respectively).

In the SE-BA3 FESEM sequence, the field for the deposited state showed mineral material covering the weave (Figure 7b). After CO_2 snow treatment, the field showed exposed filament bundles and irregular surface morphology (Figure 7c). No transverse filament discontinuities were visible in the field for the treated specimen. In the field for LN-BA3 in the treated state, separated fibre bundles and exposed fibrillar features were visible (Figure 7f). For the AL-BA3 sequence, the field for the deposited state contained mineral aggregates on the weave (Figure 7h), whereas after treatment, less mineral material was visible and the fibre morphology in this field resembled that of the clean textile reference (Figure 7i).

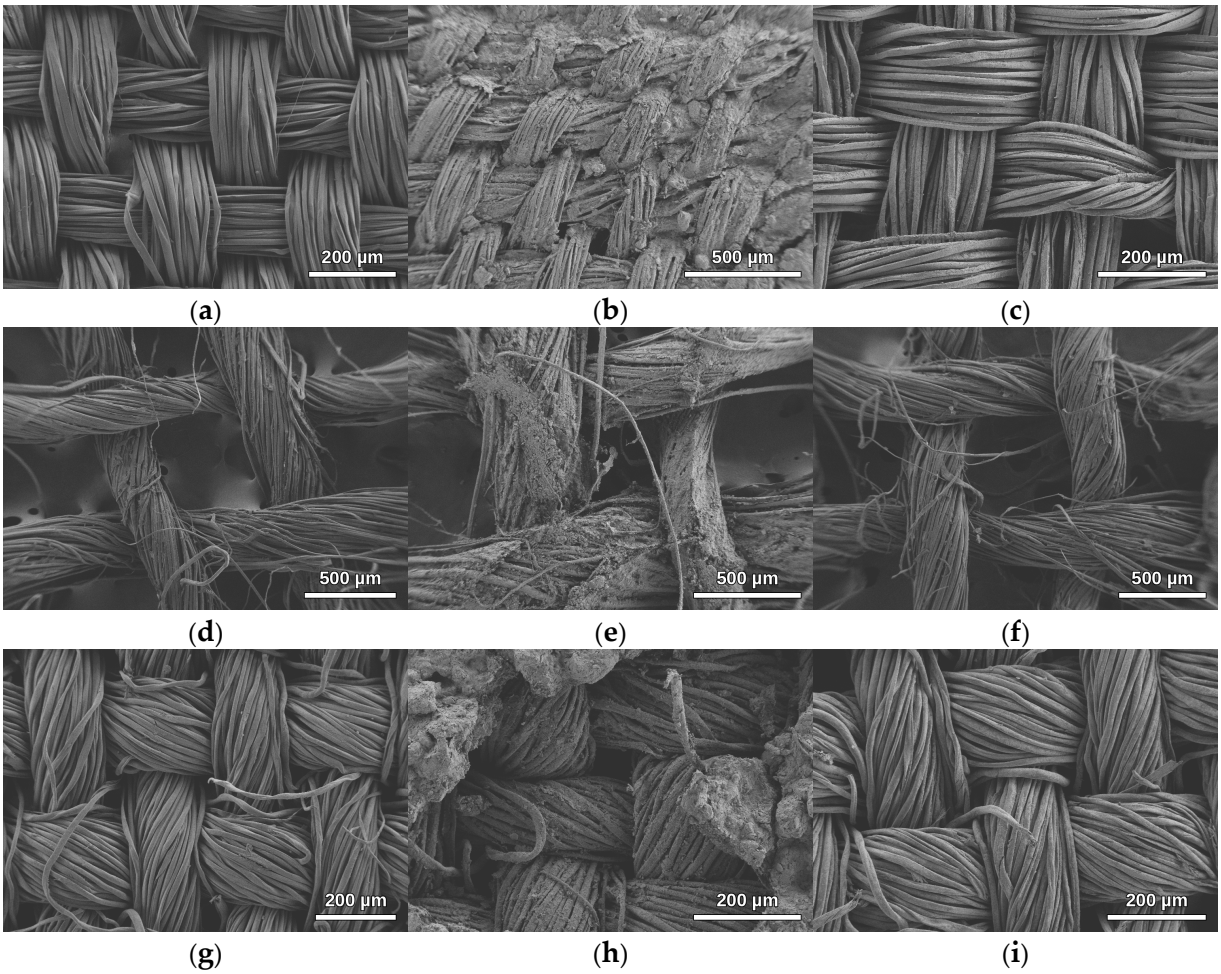


Figure 7. Comparison of FESEM results for selected fields of the red clay textile systems across M0, M1, and M2. (**a**–**c**) silk, SE-BA3; (**d**–**f**) linen, LN-BA3; (**g**–**i**) cotton, AL-BA3. Within each row, the panels show the clean textile reference, the untreated as-deposited reference and the specimen treated with configuration 3, which correspond to separate specimens. Uncoated specimens were examined at 1.00 kV using the SE2 detector, with working distances ranging from 3.1 to 3.5 mm according to the image.

In the SE-AM3 FESEM sequence, the field for the deposited state showed film-like material over the weave (Figure 8b), whereas in the treated state, discontinuous surface deposits remained and the filaments appeared separated within the yarns, producing longitudinal striations without transverse breaks (Figure 8c). These striations were not visible in the corresponding reference field (Figure 8a). In the LN-AM3 sequence, the field for the treated state showed exposed fibre bundles and fibrillar surface features (Figure 8f). However, similar fibrillar features were also visible in the linen reference field (Figure 8d), meaning that they could not be attributed exclusively to the treatment. In the AL-AM3 sequence, the field for the deposited state showed film-like coverage (Figure 8h), while in the treated state, exposed yarn bundles, fibrillated surface features and broken fibre ends were observed, indicating localised damage to individual surface fibres (Figure 8i).

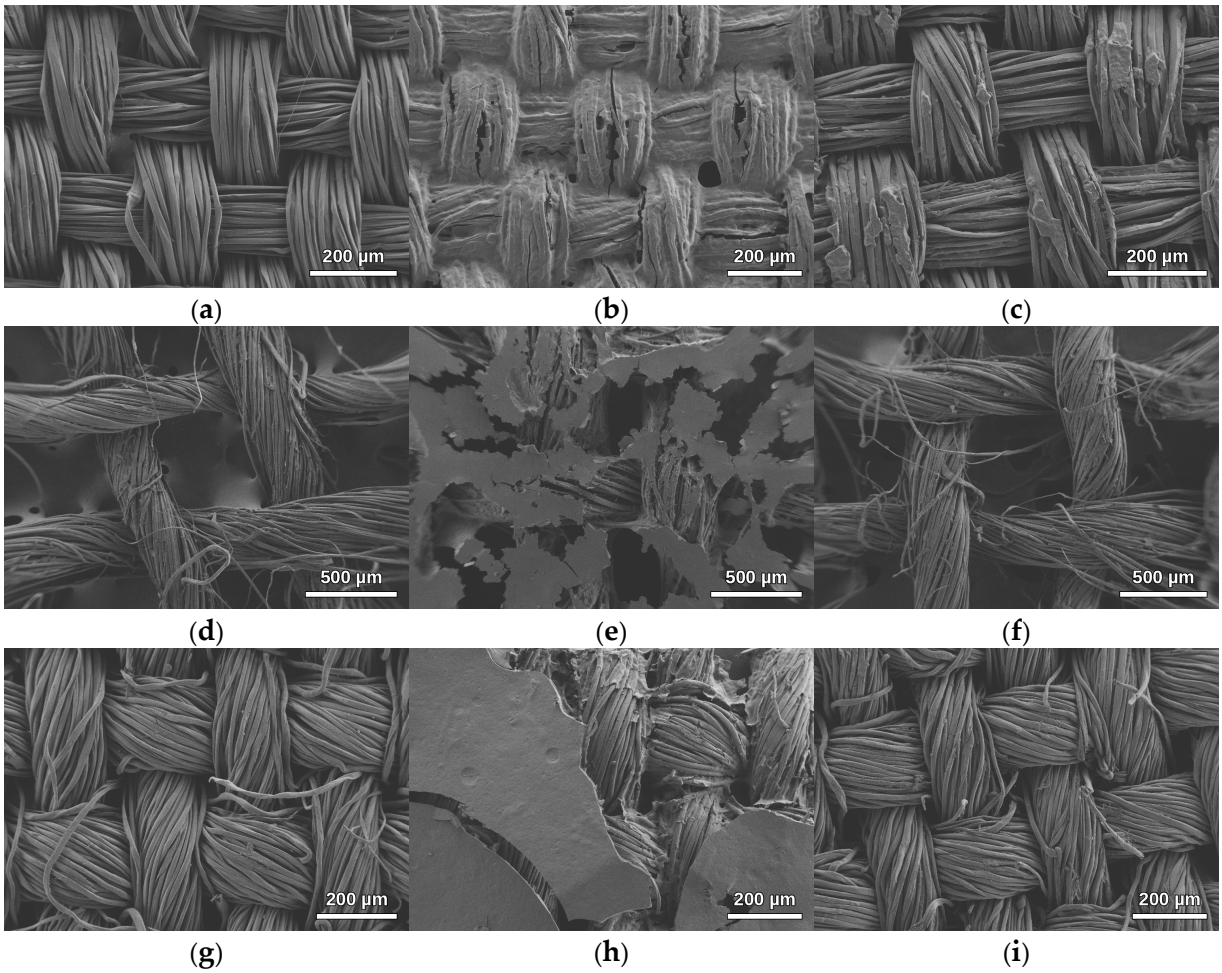


Figure 8. FESEM results for selected fields of the starch textile systems, across M0, M1, and M2: (**a**–**c**) silk, SE-AM3; (**d**–**f**) linen, LN-AM3; (**g**–**i**) cotton, AL-AM3. Within each row, the panels show the clean textile reference, the untreated as-deposited reference and the specimen treated with configuration 3, which correspond to separate specimens. Uncoated specimens were examined at 1.00 kV using the SE2 detector, with working distances ranging from 3.1 to 3.5 mm depending on the image. Panels (**a**), (**d**), and (**g**) reproduce the clean textile reference fields shown in Figures 7a, 7d and 7g, respectively, since the same reference was used for each textile.

4. Discussion

For the configurations tested, the response to CO_2 snow treatment depended mainly on the nature of the deposit. The particulate red clay was expressed mainly through visible deposit displacement, chromatic recovery and residual mineral particles, whereas the starch film, with its low chromatic contrast, was better characterised through gloss, wetting behaviour, microscopy and qualitative ATR-FTIR comparisons. Within each deposit, the response also varied among the three textiles.

4.1. Deposit-Specific Response Profiles

The clay systems showed pronounced visible and chromatic changes, consistent with the particulate nature of the mineral deposit and with the detachment or displacement of particles and aggregates by the jet. The extent of colour recovery differed among substrates. In linen, LN-BA2 and LN-BA3 approached the initial colour more closely than LN-BA1, whereas visible chromatic differences from the clean state remained in silk and cotton. The lower recovery of b* in all specimens showing chromatic recovery suggests that a

reddish and yellowish contribution of the mineral deposit persisted after the lightness had partly recovered.

The response for the red clay broadly supported the capacity of CO_2 snow jets to remove particulate matter from fibrous surfaces, as reported by Mašková et al. [10,18]. These authors found that particles could be displaced from exposed fibres and inter-fibre spaces in papers and uncoated cellulosic textiles. The present observations add a comparison between two cellulosic textiles and proteinaceous silk, using a controlled mineral deposit with a marked chromatic response. They do not establish performance equivalent to that reported in prior studies, since the equipment, jet configuration, contaminants, substrates, and application procedures differed.

Starch produced a different response. Its low chromatic contrast was accompanied by clearer changes in gloss, wetting behaviour, the distribution of the residual film and local surface morphology, together with qualitative ATR-FTIR comparisons at selected contact sites. Assessing these indicators together follows the approach of previous studies of enzymatic starch removal, which also considered residual material, colour and fibre changes [6,7].

Mechanical fracture and interfacial debonding are plausible contributors to starch-film disruption under CO_2 snow projection. Differential thermal contraction and changes in film moisture may also contribute, but their roles were not determined experimentally.

This dependence on the textile, the deposit and the treatment conditions is consistent with previous studies of particulate removal from paper and uncoated cellulose textiles with CO_2 snow [10,18] and with research on soot removal from textiles through solid CO_2 blasting [17].

4.2. Analytical Concordance Across Spatial Scales

At the macroscopic scale, visual observation and colourimetry showed concordant changes in the red clay systems. Areas with reduced visible clay coverage corresponded with chromatic recovery towards M0. In the starch systems, the smaller chromatic changes contrasted with a more differentiated surface response, consistent with the lower colour contrast and film-forming behaviour of this deposit. Recent work on soot-soiled silk has similarly shown that colourimetric estimates do not always correspond to the residual soiling visible in micrographs [29]. Colour measurements were therefore interpreted here as indicators of appearance change, rather than as direct measurements of the amount of deposit removed.

Gloss reflected the combined influence of fibre orientation, weave geometry, surface roughness and deposit distribution [30]. Post-treatment gloss at 85° was below the clean value in 16 of the 18 specimens. This decrease may reflect residual deposit, differences in fibre orientation or weave geometry, local morphological features, or a combination of these. Their respective contributions cannot be separated in the present design.

Wetting behaviour reflects the interaction of the surface with liquid water. In cotton, the high initial contact angle and long absorption time of the clean fabric suggest that residual hydrophobic substances may not have been fully removed by the prewash. The largest change in wetting occurred between the clean and deposited states, before treatment, so the difference between the clean and treated states cannot be attributed to the CO_2 snow treatment alone.

ATR-FTIR supplied complementary qualitative evidence from selected contact sites. Separate specimens, heterogeneous deposit coverage and overlapping bands prevented quantitative estimates of residual deposit or removal [28].

Digital microscopy related the distribution of the deposit and the weave spacing to the macroscopic changes, while FESEM resolved residual particles, film-like coverage, exposed

filament bundles, fibrillar features, striations and broken fibre ends in the selected fields. Differences between the two scales reflected the area and surface component represented by each technique.

The temperature on the reverse side fell to 0.7 °C only under direct impact of the jet and remained between 8 and 10 °C during sweeping, rising rapidly towards ambient once the jet moved away. Both values are below the dew point of the laboratory atmosphere (approximately 13.9 °C at 25 °C and 50% RH), and the exposed face, although not measured, was likely colder than the reverse. These temperatures indicate a risk of transient condensation, although condensation and frost were not monitored directly. Condensed water can carry fine clay particles into the fibre structure, rehydrate the starch film and favour redeposition, and it may account for part of the changes in wetting behaviour. Because CO_2 dissolves in condensed water to form carbonic acid, surface acidification was a possible risk. No persistent post-treatment acidification was detected at the tested sites, although transient changes during application cannot be excluded. A coaxial flow of dry gas has been proposed to limit condensation during CO_2 snow cleaning [13].

4.3. Contribution to the Assessment of Textile Cleaning

The observations supported partial deposit reduction, with residual material remaining in the analysed fields. In the linen–starch series, LN-AM3 exhibited the 85° gloss value closest to its own clean state, but this observation alone does not establish the greatest deposit removal. In the linen–clay series, both the 4 and 5 bar configurations showed greater chromatic recovery than the 2 bar configuration.

Lower gloss and local morphological differences accompanied the observed reduction in deposit coverage. Broken fibre ends were visible in the selected cotton–starch field. Their origin and prevalence cannot be established from the unmatched fields and available controls. Because each configuration was represented by one specimen, the results do not establish optimal parameters or a reproducible efficacy–risk relationship.

4.4. Transferability and Limitations

The study provides a comparison of the response of silk, cotton and linen to CO_2 snow cleaning of a particulate and a film-forming deposit, documented through complementary optical, surface, spectroscopic and morphological measurements. Its exploratory design, however, limits how far these results can be generalised. Each configuration was applied to a single specimen, the configurations were not arranged as a factorial matrix, and no clean textile was exposed to the CO_2 snow configurations. Differences between the clean and treated states may therefore reflect residual deposit, the mechanical action of the jet, transient cooling and associated condensation, or a combination of these, which the present design does not allow to be separated. Deposit loads and the mass removed were not determined gravimetrically, and the red clay was not characterised mineralogically, so colour recovery describes an optical change rather than the amount of deposit removed.

These limitations define the next steps of this research. Replicated specimens and a clean textile exposed to the same configurations would allow treatment effects to be separated from residual deposit, while the measurement of yarn displacement and mechanical characterisation would make the assessment of alteration quantitative. The analysis can also be extended to defined nozzle trajectories, post-treatment ageing and comparison with established cleaning procedures. Future work should also incorporate reproducible protocols for deposit application and quantified deposit loads, consistent with recent approaches to the preparation of soiled heritage mock-ups for comparative cleaning studies [31]. These studies support the methodological feasibility of the proposed extensions, although the results obtained from different deposits and substrates cannot be transferred

directly to fibrous heritage materials. Aged, dyed, finished, previously treated, and structurally modified textiles can be incorporated as differentiated material systems within the same experimental approach.

5. Conclusions

Under the tested configurations, optical and microscopic observations supported partial reduction of the deposits, with residual material remaining in the analysed fields. The findings describe individual textile–deposit systems and do not establish a general relationship between removal, pressure and application time.

Post-treatment gloss at 85° was below the clean value in 16 of the 18 specimens. Local morphological differences included separated silk filaments and broken cotton fibre ends. These observations identify potential conservation concerns, but the present design does not establish their origin or prevalence.

Within the limits of this exploratory study, the results underline the importance of adjusting the treatment parameters to each textile and deposit. The search for a working range that removes deposits effectively while keeping the alteration of the fibres within acceptable limits therefore needs to be continued. Further systematic study of the interplay between pressure, exposure time and nozzle trajectory will be required to identify the conditions that combine efficient cleaning with the preservation of the textile.

Supplementary Materials: The following supporting information can be downloaded at: https://www.mdpi.com/article/10.3390/app162110923/s1. Table S1: Individual CIELAB readings of the treated specimens at M0, M1 and M2; Table S2: Colour differences of the treated specimens relative to M0; Table S3: Mean CIELAB coordinates of the treated specimens at M0, M1 and M2; Table S4: Individual gloss readings of the treated specimens at M0, M1 and M2; Table S5: Mean gloss values of the treated specimens at M0, M1 and M2; Table S6: Surface pH readings; Table S7: Mean water droplet response.

Author Contributions: Conceptualization, M.P.W.-C. and V.S.-C.; methodology, M.P.W.-C., V.S.-C. and L.O.-C.; formal analysis, L.O.-C., M.P.W.-C. and V.S.-C.; investigation, M.P.W.-C., V.S.-C., L.O.-C. and S.V.-P.; resources, M.P.W.-C., V.S.-C., L.O.-C. and S.V.-P.; writing—original draft preparation, M.P.W.-C. and V.S.-C.; writing—review and editing, M.P.W.-C., V.S.-C., L.O.-C. and S.V.-P.; supervision, V.S.-C. and L.O.-C.; project administration, V.S.-C.; funding acquisition, V.S.-C. All authors have read and agreed to the published version of the manuscript.

Funding: This research was funded by MICIU/AEI/10.13039/501100011033 and by ERDF/EU, grant number PID2023-148231OB-I00.

Institutional Review Board Statement: Not applicable.

Informed Consent Statement: Not applicable.

Data Availability Statement: Individual colour, gloss and surface pH readings, together with the retained mean wetting values, are provided in the Supplementary Materials. Other data are available from the corresponding authors upon reasonable request.

Conflicts of Interest: The authors declare no conflicts of interest.

References

1. Tímár-Balázsy, Á. Wet Cleaning of Historical Textiles: Surfactants and Other Wash Bath Additives. *Stud. Conserv* **2000**, *45*, 46–64. [CrossRef]
2. Guglielmi, V.; Comite, V.; Lombardi, C.A.; Bergomi, A.; Boanini, E.; Bonomi, R.; Monfasani, E.; Sassi, L.; Borelli, M.; Fermo, P. Restoration of a Textile Artefact: A Comparison of Cleaning Procedures Applied to a Historical Tapestry from the Quirinale Palace (Rome). *Appl. Sci.* **2023**, *13*, 2669. [CrossRef]

3. Alván, M.J.; Candiotti, S.; Flores, E.; Charca, S. Impact of Washing and Aging Process on the Physical and Mechanical Properties of Pre-Hispanic Fabrics Found in the Museum of Site and Archeological Sanctuary of Pachacamac, Perú. *J. Cult. Herit.* **2024**, *67*, 360–367. [CrossRef]
4. Brockmann, N.; Sicken, A.; Krüger, J. Effects of Laser Cleaning on the Condition of Different Silk Model Samples Using Varying Wavelengths and Pulse Durations. *Herit. Sci.* **2024**, *12*, 34. [CrossRef]
5. Uring, P.; Chabas, A.; Alfaro, S. Dust Deposition on Textile and Its Evolution in Indoor Cultural Heritage. *Eur. Phys. J.* **2019**, *134*, 255. [CrossRef]
6. Ahmed, H.E.; Kolisis, F.N. An Investigation into the Removal of Starch Paste Adhesives from Historical Textiles by Using the Enzyme α-Amylase. *J. Cult. Herit.* **2011**, *12*, 169–179. [CrossRef]
7. Tortora, M.; Gherardi, F.; Ferrari, E.; Colston, B. Biocleaning of Starch Glues from Textiles by Means of α-Amylase-Based Treatments. *Appl. Microbiol. Biotechnol.* **2020**, *104*, 5361–5370. [CrossRef] [PubMed]
8. Šahinbaşkan, B.Y.; Kahraman, M.V. Desizing of Untreated Cotton Fabric with the Conventional and Ultrasonic Bath Procedures by Immobilized and Native α-Amylase. *Starch/Staerke* **2011**, *63*, 154–159. [CrossRef]
9. Al-Emam, E.; Cremonesi, M.; Ortega Saez, N.; Soenen, H.; Janssens, K.; Van der Snickt, G. Exploring the Potential of Polyvinyl Alcohol–Borax-Based Gels for the Conservation of Historical Silk Fabrics by Comparative Cleaning Tests on Simplified Model Systems. *Gels* **2026**, *12*, 97. [CrossRef] [PubMed]
10. Mašková, L.; Smolík, J.; Vávrová, P.; Neoralová, J.; Součková, M.; Novotná, D.; Jandová, V.; Ondráček, J.; Ondráčková, L.; Křížová, T.; et al. Carbon Dioxide Snow Cleaning of Paper. *Herit. Sci.* **2021**, *9*, 145. [CrossRef]
11. Ferrari, M.; Mazzoli, R.; Morales, S.; Fedi, M.; Liccioli, L.; Piccirillo, A.; Cavaleri, T.; Oliva, C.; Gallo, P.; Borla, M.; et al. Enzymatic Laundry for Old Clothes: Immobilized Alpha-Amylase from Bacillus Sp. for the Biocleaning of an Ancient Coptic Tunic. *Appl. Microbiol. Biotechnol.* **2017**, *101*, 7041–7052. [CrossRef] [PubMed]
12. Sherman, R. Carbon Dioxide Snow Cleaning Applications. In *Developments in Surface Contamination and Cleaning: Applications of Cleaning Techniques*; Kohli, R., Mittal, K.L., Eds.; Elsevier: Amsterdam, The Netherlands, 2019; Volume 11, pp. 97–115. [CrossRef]
13. Shockey, L.H., Jr. Blow It off. Moving beyond Compressed Air with Carbon Dioxide Snow. *AIC Objects Spec. Group Postprints* **2009**, *16*, 13–14.
14. Vega-Bosch, A.; Santamarina-Campos, V.; Osete-Cortina, L.; Sánchez-Pons, M.; Bosch-Roig, P. Efficient and Sustainable Cleaning: A Comparative Analysis of Cryogenic Technology. *Appl. Sci.* **2024**, *14*, 6591. [CrossRef]
15. Spur, G.; Uhlmann, E.; Elbing, F. Dry-Ice Blasting for Cleaning: Process, Optimization and Application. *Wear* **1999**, *233–235*, 402–411. [CrossRef]
16. Stoveland, L.P.; Frøysaker, T.; Stols-Witlox, M.; Grøntoft, T.; Steindal, C.C.; Madden, O.; Ormsby, B. Evaluation of Novel Cleaning Systems on Mock-Ups of Unvarnished Oil Paint and Chalk-Glue Ground within the Munch Aula Paintings Project. *Herit. Sci.* **2021**, *9*, 144. [CrossRef]
17. Grønlund, M. An Evaluation of Solid Carbon Dioxide (CO_2) Blasting as a Cleaning Method to Remove Soot from Textiles after Smouldering Fire and Fire, with the Possibility to Transfer the Method to Historical Textiles within a Museum Context. *CeROArt* **2014**. [CrossRef]
18. Mašková, L.; Smolík, J.; Vávrová, P.; Neoralová, J.; Novotná, D.; Jandová, V.; Ondráček, J.; Kocová, K.; Marešová, A.; Zedníková, M.; et al. CO_2 Snow Microblasting of Submicron Particles from Cellulose-Based Cultural Heritage Objects: Comparison with Traditional Dry Cleaning Methods. *J. Cult. Herit.* **2024**, *70*, 1–11. [CrossRef]
19. Vega-Bosch, A.; Osete-Cortina, L.; Santamarina-Campos, V.; Dolz-Ruiz, V. Effectiveness and Environmental Performance of Cryogenic CO_2 Cleaning for Graffiti Removal from Contemporary Out-Door Metallic Sculptures. *J. Cult. Herit.* **2026**, *80*, 291–301. [CrossRef]
20. Chillè, C.; Rossignoli, G.; Nagasawa, T.; Osticioli, I.; Agresti, J.; Siano, S.; Ciofini, D. Laser Cleaning of Artificially Soiled Cotton Fabric: Assessment of Surface Chemical Effects. *J. Cult. Herit.* **2023**, *64*, 1–11. [CrossRef]
21. Havlová, M.; Kocová, K.; Neoralová, J.; Novotná, D.; Vávrová, P.; Mašková, L. PVC Cleaning via Different Methods: Comparison of Laser and CO_2 Snow. In *Lasers in the Conservation of Artworks XIII: Proceedings of the International Conference on Lasers in the Conservation of Artworks XIII (LACONA XIII), Florence, Italy, 12–16 September 2022*; Siano, S., Ciofini, D., Eds.; CRC Press: London, UK, 2023; pp. 183–187. [CrossRef]
22. CryoSnow GmbH. CO_2 Snow Blasting Machine SJ-5. Available online: https://www.cryosnow.com/en/products/manual-blasting-machines/co2-snow-blasting-machine-sj-5/ (accessed on 29 July 2026).
23. CryoSnow GmbH. Nozzles for Blasting Pistol JP-5: Flat Nozzle FN-5-10x1_5. Available online: https://www.cryosnow.com/en/accessories/nozzles/nozzles-for-blasting-pistol-jp-5/ (accessed on 29 July 2026).
24. *UNE-EN 15886:2011*; Conservation of Cultural Property. Test Methods. Colour Measurement of Surfaces. AENOR: Madrid, Spain, 2011.
25. Rota, E.; Bozzi, C.; Cremonesi, P.; Lucchini, A. Study of the Best Methodology for Measuring Surface PH of Linen Canvas. *Stud. Conserv.* **2021**, *66*, 313–320. [CrossRef]

26. *UNE-EN 15802*; Conservation of Cultural Property. Test Methods. Determination of Static Contact Angle. AENOR: Madrid, Spain, 2010.
27. *UNE-EN ISO 2813:2015*; Paints and Varnishes. Determination of Gloss Value at 20°, 60° and 85° (ISO 2813:2014). AENOR: Madrid, Spain, 2015.
28. Cutajar, J.D.; Steindal, C.C.; Caruso, F.; Joseph, E.; Frøysaker, T. Spectral- and Image-Based Metrics for Evaluating Cleaning Tests on Unvarnished Painted Surfaces. *Coatings* **2024**, *14*, 1040. [CrossRef]
29. Cremonesi, M.; Pastorelli, G.; Yang, N.; Al-Emam, E.; Martinelli, E.; Comelli, D.; Dal Fovo, A.; Fontana, R.; Cicchi, R.; Ortega Saez, N.; et al. Evaluating Cleaning Efficacy by Image-Based Machine Learning: Case Study of Soot Removal from Silk. *npj Herit. Sci.* **2026**, *14*, 393. [CrossRef]
30. Akgun, M.; Becerir, B.; Alpay, H.R. The Effect of Fabric Constructional Parameters on Percentage Reflectance and Surface Roughness of Polyester Fabrics. *Text. Res. J.* **2012**, *82*, 700–707. [CrossRef]
31. Yang, N.; Cremonesi, M.; Markevicius, T.; Dal Fovo, A.; Shumikhin, K.; Ducoli, E.; Rocha Pires, C.; Fontana, R.; Van Der Voort, P.; Leus, K.; et al. The Reproduction of Fire-Born Soot for Comparative Cleaning Tests on Heritage Objects. *npj Herit. Sci.* **2025**, *13*, 593. [CrossRef] [PubMed]

Disclaimer/Publisher's Note: The statements, opinions and data contained in all publications are solely those of the individual author(s) and contributor(s) and not of MDPI and/or the editor(s). MDPI and/or the editor(s) disclaim responsibility for any injury to people or property resulting from any ideas, methods, instructions or products referred to in the content.